Persistent random walk in a honeycomb structure: Light transport in foams

MirFaez Miri[1,2] and Holger Stark[2]
[1]*Institute for Advanced Studies in Basic Sciences, Zanjan 45195-159, Iran*
[2]*Universität Konstanz, Fachbereich Physik, D-78457 Konstanz, Germany*
(Received 19 December 2002; published 16 September 2003)

We study light transport in a honeycomb structure as the simplest two-dimensional model foam. We apply geometrical optics to set up a persistent random walk for the photons. For three special injection angles of 30°, 60°, and 90° relative to a hexagon's edge, we are able to demonstrate by analytical means the diffusive behavior of the photons and to derive their diffusion constants in terms of intensity reflectance, edge length, and velocity of light. Numerical simulations reveal an interesting dependence of the diffusion constant on the injection angle in contrast to the usual assumption that in the diffusive limit the photon has no memory for its initial conditions. Furthermore, for injection angles close to 30°, the diffusion constant does not converge to the value at 30°. We explain this observation in terms of a two-state model.

DOI: 10.1103/PhysRevE.68.031102 PACS number(s): 05.40.Fb, 05.60.−k, 82.70.Rr, 42.25.Dd

I. INTRODUCTION

Diffusing photons [1–3] in a multiply scattering medium, such as conventional colloidal suspensions or thick aligned nematic liquid crystals, provide information about the static and dynamic properties of an opaque system, as recently developed techniques such as diffusing-wave spectroscopy [4,5] and diffuse-transmission spectroscopy [6] have demonstrated.

A light beam from a monomode laser is multiply scattered either from particles in the case of colloidal suspensions or from thermal fluctuations of the local optical axis in nematic liquid crystal. It travels through the medium along various paths which interfere with each other at the detector giving rise to a highly irregular intensity or speckle pattern [2,7]. Since in leading order the paths are statistically independent from each other [7], configurational averaging results in a smooth mean intensity distribution that obeys a diffusion equation. This is the basis of the random walk picture for diffusing photons.

Note that speckle patterns can be explained in the limit of diffusing photons by attaching a phase factor to the photons which grows, like in a plane wave, with the length of the photon path. All phase factors of the different photon paths add up providing a strongly fluctuating intensity pattern on the detecting screen. This is the well-known speckle pattern. Conventional diffusing-wave spectroscopy then measures the temporal intensity autocorrelation function of one speckle by replacing, as usual, the ensemble average by an average in the time domain [4].

Recent experiments have applied diffusing-wave spectroscopy to cellular structures such as foams which consist of air bubbles separated by liquid films [8–13]. This suggests that the model for the photon transport based on the random walk picture is still valid. However, there is a debate in literature about the main mechanism underlying the random walk [10]. Relatively dry foam consists of cells separated by thin liquid films. Three of them meet in the Plateau borders which then define the tetrahedral vertices [14]. One suggestion is that light scattering from the Plateau borders is the main origin of the random walk. On the other hand, since the cells are much larger than the wavelength of light, one can employ geometrical optics and follow a light beam or photon as it is reflected by the liquid films with a probability r called the intensity reflectance. This naturally leads to a random walk of the photons in space.

In this paper we concentrate on the second mechanism based on geometrical optics. Furthermore, instead of a disordered foam, we choose the honeycomb structure that always served as the simplest two-dimensional model foam [15]. In the Princen-Prud'Homme model, e.g., it has been used to access the rheological properties of foams [16]. Implementing the rules from geometrical optics for transmittance and reflectance of light results in a persistent random walk. The concept of random walks has extensively been studied and applied to different areas in physics [17,18]. Especially persistent random walks, where the walker remembers its direction from the previous step, are employed in turbulent diffusion [19], polymers [20], diffusion in solids [21], and in general transport mechanisms [22–24].

In the honeycomb structure, the classical one-dimensional persistent random walk arises when the photons move perpendicular to a cell edge of the honeycomb. It is known as a second-order Markov chain for which an analytical solution exists [17]. In addition, we identify two further, analytically solvable cases, where the photon moves with an angle of 30° or 60° relative to a cell edge. As we will demonstrate, they correspond to Markov chains of 12th order. Nevertheless, we are able to proof the diffusive behavior in the long-time limit and to determine the respective diffusion constants. Numerical studies for an arbitrary angle of incidence φ reveal a surprising dependence of the diffusion constant on φ. They also motivate a fourth, analytically solvable case based on a two-state model, a formalism well established in the theory of random walks [17]. Thus, we demonstrate that the random walk on a honeycomb structure based on rules introduced from geometrical optics is a highly interesting model system.

Our paper is organized as follows. In Sec. II we introduce the possible photon paths in a honeycomb structure and identify special cases whose analytic solutions we illustrate in Sec. III. The numerical treatment and its results are reported in Sec. IV. The two-state model that explains a special fea-

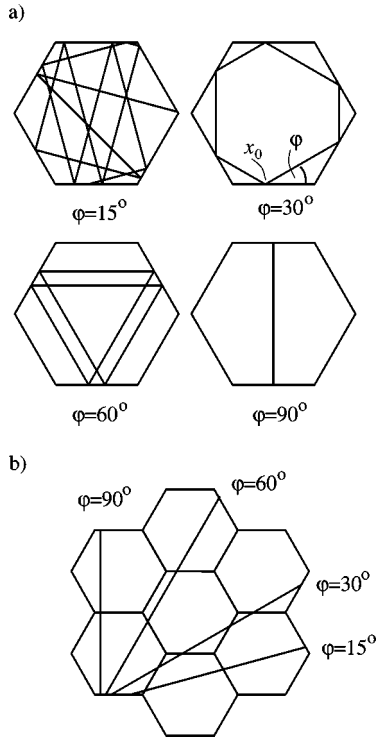

FIG. 1. (a) Different photon paths in a hexagon with completely reflecting edges for different angles of incidence φ, measured relative to the edge, and starting point x_0 on the edge. The paths for $\varphi=30°$ and 60° are closed. The path for 90° is one dimensional. (b) The representation of the paths as straight lines in a honeycomb structure evolves when the complete hexagon is reflected at the edge where the path is reflected.

ture of the numerical results follows in Sec. V. We close with conclusions in Sec. VI.

II. PHOTON PATHS IN A HONEYCOMB STRUCTURE

In the following we model the photon paths in a honeycomb structure as a random walk with rules motivated by geometrical optics, i.e., an incoming light beam is reflected from an edge with a probability r, called the intensity reflectance, or traverses the edge with a probability $t=1-r$, called the transmittance. The unit cell of the honeycomb is a hexagon which, recently, has received much attention as special type of a polygonal billard [25] and in models of microlasers and microresonators for visible light [26]. Hexagons are termed pseudointegrable since they are between classical integrable and chaotic systems [25]. They do not possess a unique set of action-angle variables, which characterize an integrable system, and neighboring beams of trajectory only split at the vertices of a hexagon unlike a fully chaotic system.

We classify the photon paths in a hexagon with completely reflecting edges ($r=1$) by the angle of incidence φ, measured relative to one of the edges, and by the starting position $x_0 l$ on the edge, where l is the edge length and $0 \leqslant x_0 \leqslant 1$ [see Fig. 1(a)]. From the geometry and symmetry of a hexagon, it is straightforward to show that each photon path is characterized by only the following three angles of incidence:

$$0° \leqslant \varphi_1 \leqslant 30°, \quad \varphi_2 = 60° - \varphi_1, \quad \text{and} \quad \varphi_3 = 60° + \varphi_1, \tag{1}$$

which leads, in general, to a nonclosed photon path with six different directions of propagation as illustrated in Fig. 1(a) for $\varphi=15°$. This can also be seen from an instructive representation of the photon path: by reflecting the hexagon at the edge from which the light ray is reflected, the photon path appears as a straight line in a honeycomb structure [see Fig. 1(b)]. The special cases of $\varphi_1=\varphi_2=30°, \varphi_3=90°$ and $\varphi_1=0°, \varphi_2=\varphi_3=60°$ give closed photon paths [see Fig. 1(a)] with a finite number of step lengths and directions. They therefore allow an analytical treatment of the random walk which takes place at intensity reflectances $r<1$. We will illustrate the calculation of the corresponding diffusion constants in the following section. The angles $\varphi_1=\varphi_2=30°$ and $\varphi_3=90°$ correspond to separate random walks in two and one dimension, respectively. However, close to $\varphi_1 \approx 30°$ they mix and can be treated in terms of a two-state model which we present in Sec. V.

When implementing the geometric optics, we assume that the intensity reflectance r and the transmittance $t=1-r$ do not depend on the angle of incidence φ and that the edges are infinitely thin so there is no lateral displacement of the transmitted light ray along the edge. In the concrete calculations, we will normalize edge length l and light velocity c to 1.

III. ANALYTICAL TREATMENT OF PHOTON TRANSPORT IN A HONEYCOMB

As already mentioned in the Introduction, the random walk on a honeycomb based on geometric optics is a persistent random walk since the new direction chosen by the photon in the $(n+1)$th step depends on the direction of the nth step. In one dimension, which in our case corresponds to an angle of incidence $\varphi=90°$ and step length $\sqrt{3}l$, the solution for the probability $P_n(x)$ of finding the random walker at location x after n steps is well known. It is determined in the framework of master equations and characteristic functions, i.e., the spatial Fourier transforms of probability distributions [17]. The persistent walk in one dimension is a second-order Markov process since $P_n(x)$ obeys a second-order linear difference equation in the discrete step index n which, in the continuous case, gives the telegrapher equation. For both equations, the long-time limit is shown to be diffusive. In our case, with step length $\sqrt{3}l$ and reflectance r, the diffusion constant amounts to

$$D(90°) = \frac{\sqrt{3}}{2} \frac{1-r}{r} lc. \tag{2}$$

In the following two sections, we will illustrate the analytical treatment of the persistent random walks for $\varphi=60°$ and 30° based on the formulation of a set of master equations and the use of characteristic functions. Since the random walks are two dimensional, the evaluation of the diffusion constants is much more elaborate.

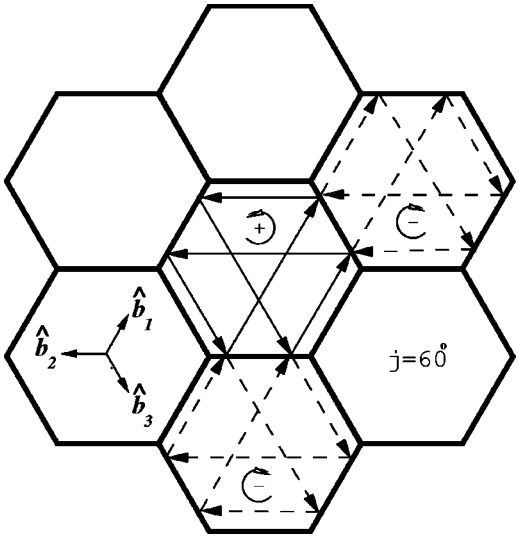

FIG. 2. Path of photons injected with an angle of $\varphi=60°$. The photons move along three directions $\hat{\boldsymbol{b}}_1$, $\hat{\boldsymbol{b}}_2$, and $\hat{\boldsymbol{b}}_3$ with a short and a long step length. By transmission to a neighboring cell, the helicity of the photon path changes.

A. Angle of incidence: $\varphi=60°$

As already mentioned in the last section, in a hexagon with totally reflecting edges ($r=1$), photons injected at an angle of $\varphi=60°$ move along a closed path generally composed of six steps (see Fig. 2). Only three directions in space, characterized by unit vectors $\hat{\boldsymbol{b}}_1$, $\hat{\boldsymbol{b}}_2$, and $\hat{\boldsymbol{b}}_3$, are assumed, and along each direction a short ($\boldsymbol{b}_{is}=b_s\hat{\boldsymbol{b}}_i$) and a long ($\boldsymbol{b}_{il}=b_l\hat{\boldsymbol{b}}_i$) step vector exists with the respective magnitudes $b_s=1.5-|0.5-x_0|$ and $b_l=1.5+|0.5-x_0|$. The average step length is thus 1.5, and it is assumed for $x_0=0.5$ where the closed path is composed of only three steps.

Note that in the central cell in Fig. 2 the photon is always reflected to the left. For partially reflecting edges ($r<1$), the photons move to a neighboring cell with the probability t. At each transmission, the photon's attribute to be reflected to the right or to the left changes (see Fig. 2). To fully characterize the status of a photon, we therefore have to introduce a helicity $\pm$ besides the position and the step vectors.

We denote by $P_n^{\pm is}(\boldsymbol{x})$ or $P_n^{\pm il}(\boldsymbol{x})$ the probability that the photon after its nth step arrives at position $\boldsymbol{x}=(x,y)$ with step vector $\boldsymbol{b}_{is}$ or $\boldsymbol{b}_{il}$ and helicity $\pm$. According to Fig. 2, we can establish a set of 12 master equations which couple the probabilities at step $n+1$ to the probabilities at step n. We only give the following first four equations:

$$
\begin{aligned}
P_{n+1}^{+1l}(\boldsymbol{x}) &= rP_n^{+3s}(\boldsymbol{x}-\boldsymbol{b}_{1l})+tP_n^{-1s}(\boldsymbol{x}-\boldsymbol{b}_{1l}),\\
P_{n+1}^{+1s}(\boldsymbol{x}) &= rP_n^{+3l}(\boldsymbol{x}-\boldsymbol{b}_{1s})+tP_n^{-1l}(\boldsymbol{x}-\boldsymbol{b}_{1s}),\\
P_{n+1}^{-1l}(\boldsymbol{x}) &= rP_n^{-2s}(\boldsymbol{x}-\boldsymbol{b}_{1l})+tP_n^{+1s}(\boldsymbol{x}-\boldsymbol{b}_{1l}),\\
P_{n+1}^{-1s}(\boldsymbol{x}) &= rP_n^{-2l}(\boldsymbol{x}-\boldsymbol{b}_{1s})+tP_n^{+1l}(\boldsymbol{x}-\boldsymbol{b}_{1s}).
\end{aligned}
\tag{3}
$$

For the description of the photon distribution in the plane, we do not need to specify the internal state (step vector and helicity) explicitly. That means we are mainly interested in the probability that the photon arrives at position $\boldsymbol{x}$ at step n,

$$
P_n(\boldsymbol{x})=\sum_{\pm,\boldsymbol{b}_{is}} P_n^{\pm is}(\boldsymbol{x})+\sum_{\pm,\boldsymbol{b}_{il}} P_n^{\pm il}(\boldsymbol{x}), \tag{4}
$$

from which we extract the first and second moments after n steps as the characteristic features of a random walk:

$$
\begin{aligned}
\langle x\rangle_n &= \int\int xP_n(x,y)dxdy,\\
\langle y\rangle_n &= \int\int yP_n(x,y)dxdy,\\
\langle (x-\langle x\rangle_n)^2\rangle_n &= \int\int (x-\langle x\rangle_n)^2P_n(x,y)dxdy,\\
\langle (y-\langle y\rangle_n)^2\rangle_n &= \int\int (y-\langle y\rangle_n)^2P_n(x,y)dxdy.
\end{aligned}
\tag{5}
$$

These moments are conveniently calculated from the Fourier transform of the probability distribution, also called characteristic function,

$$
P_n(\boldsymbol{k})=\int\int e^{i\boldsymbol{k}\cdot\boldsymbol{x}}P_n(x,y)dxdy, \tag{6}
$$

from which the moments follow as

$$
\langle x^{m_1}y^{m_2}\rangle=(-i)^{m_1+m_2}\left.\frac{\partial^{m_1+m_2}P_n(\boldsymbol{k})}{\partial k_x^{m_1}\partial k_y^{m_2}}\right|_{\boldsymbol{k}=\boldsymbol{0}}, \tag{7}
$$

where $\boldsymbol{k}=(k_x,k_y)$ and m_1, m_2 are positive integers including zero.

In the following we illustrate how we compute the characteristic function $P_n(\boldsymbol{k})$. We start from the set of coupled master equations (3), take its Fourier transform and write it in a compact form as

$$
(-\mathcal{E}\boldsymbol{1}+\boldsymbol{M})\boldsymbol{P}_n=0, \tag{8}
$$

where

$$
\boldsymbol{P}_n=(P_n^{+1l}(\boldsymbol{k}),P_n^{+1s}(\boldsymbol{k}),P_n^{-1l}(\boldsymbol{k}),P_n^{-1s}(\boldsymbol{k}),\ldots)^t \tag{9}
$$

is a 12-component vector containing the step-dependent probability distributions. The shift operator $\mathcal{E}$ acts on the step index n as follows:

$$
\mathcal{E}P_n^{\pm il}(\boldsymbol{k})=P_{n+1}^{\pm il}(\boldsymbol{k}), \tag{10}
$$

where $\mathcal{E}-1$ corresponds to the time derivative in the continuous case. The symbol $\boldsymbol{M}$ denotes a 12×12 matrix that depends on the reflectance r and exponential factors such as $\exp(i\boldsymbol{k}\cdot\boldsymbol{b}_{il})$, which result from the step vectors in Eqs. (3). We list the complete $\boldsymbol{M}$ in the Appendix.

In analogy to the solution of a homogeneous system of linear equations, we know that every single probability distribution obeys the same linear equation: $\det(\boldsymbol{M}$

$-\mathcal{E}\mathbf{1})P_n^{+1l}(\boldsymbol{k})=0$, where det means determinant. Therefore the sum $P_n(\boldsymbol{k})$, defined in Eqs. (4) and (6), also obeys

$$\det(\boldsymbol{M}-\mathcal{E}\mathbf{1})P_n(\boldsymbol{k})=0. \tag{11}$$

We used the algebraic program MATHEMATICA to calculate the determinant of the 12×12 matrix $\boldsymbol{M}-\mathcal{E}\mathbf{1}$. It results in an even polynomial of degree 12 in the shift operator $\mathcal{E}$, which is equivalent to the characteristic polynomial of the matrix $\boldsymbol{M}$. With definition (10) for $\mathcal{E}$, we obtain from Eq. (11) the master equation

$$\sum_{i=0}^{i=6} m_{2i}P_{n+2i}(\boldsymbol{k})=0, \tag{12}$$

where the coefficients m_{2i} of the characteristic polynomial of $\boldsymbol{M}$ are listed in the Appendix. We add two comments. First, Eq. (12) is a 12th-order linear difference equation for $P_n(\boldsymbol{k})$ indicating that the corresponding random walk is a 12th order Markov chain. In the continuum limit, it would correspond to a linear partial differential equation with time derivatives up to the 12th order. Second, due to the normalization of the probability distribution $[P_n(\boldsymbol{k}=\mathbf{0})=1]$, we find

$$\sum_{i=0}^{i=6} m_{2i}=0, \tag{13}$$

and can therefore identify ±1 as two eigenvalues of $\boldsymbol{M}$.

We do not make an attempt to determine $P_n(\boldsymbol{k})$ completely. Instead we are interested in the long-time limits of its first two moments. Taking first derivatives of Eq. (12) with respect to $\boldsymbol{k}$ and using Eq. (7), we find a master equation for the mean displacement along the x direction,

$$\sum_{i=0}^{i=6} m_{2i}|_{\boldsymbol{k}=0}\langle x\rangle_{n+2i}=0 \tag{14}$$

and the equivalent result for the y direction. To arrive at Eq. (14), we used $\partial m_{2i}/\partial\boldsymbol{k}|_{\boldsymbol{k}=\mathbf{0}}=\mathbf{0}$ since the step vectors $\boldsymbol{b}_{is}$ and $\boldsymbol{b}_{il}$ add up to zero. To solve Eq. (14), we insert the ansatz $\langle x\rangle_n\propto z^n$, which readily results in the characteristic equation for $\boldsymbol{M}$ at $\boldsymbol{k}=\mathbf{0}$. We already know the two eigenvalues ±1, the others are listed in the Appendix. Their magnitudes are always smaller than one. We can therefore conclude that in the long-time limit or for large n

$$\langle x\rangle_n=\langle y\rangle_n=0. \tag{15}$$

The mean-square displacement along x obeys

$$\sum_{i=0}^{i=6}\left(m_{2i}|_{\boldsymbol{k}=\mathbf{0}}\langle x^2\rangle_{n+2i}-\left.\frac{\partial^2 m_{2i}}{\partial k_x^2}\right|_{\boldsymbol{k}=\mathbf{0}}\right)=0 \tag{16}$$

and an equivalent equation is valid along y. Note that Eq. (16) corresponds to Eq. (14) but now with an inhomogeneity. Since we already know the solutions of the homogeneous equation, they decay to zero or give a constant of the order of 1 in the long-time limit, we just need a special solution for which we make the ansatz $\langle x^2\rangle_n=an$. The constant a is easily found from Eq. (16) and we obtain in the long-time limit

$$\langle x^2\rangle_n=\frac{1}{S_2}\left.\frac{\partial^2 S_1}{\partial k_x^2}\right|_{\boldsymbol{k}=\mathbf{0}} n, \tag{17}$$

where $S_2=\Sigma_{i=1}^{i=6}2i\ m_{2i}$ and the derivative of $S_1=\Sigma_{i=1}^{i=5}m_{2i}$ both at $\boldsymbol{k}=\mathbf{0}$ are given in the Appendix and Eq. (13) was used. For large values of n, the time for n steps is $\tau=1.5ln/c$, where $1.5l$ is the average step length. Returning to physical units, we obtain the diffusive behavior for the mean-square displacements

$$\langle x^2\rangle=2D_x\tau \quad\text{and}\quad \langle y^2\rangle=2D_y\tau, \tag{18}$$

and the diffusion constants read

$$D(60°)=D_x(60°)=D_y(60°)=\frac{1}{2}\frac{1-r}{r}lc. \tag{19}$$

As expected, the diffusion is isotropic. Note that although the single-step lengths depend on the starting position x_0 on the edge of a hexagon, only their average appears in the final, reasonable result.

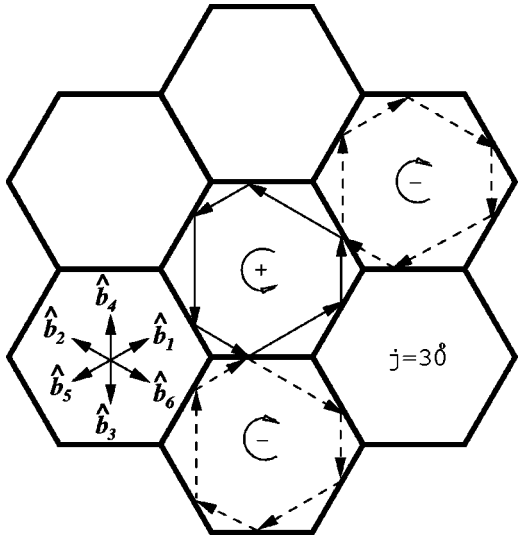

FIG. 3. Path of photons injected with an angle of $\varphi=30°$. The photons move along six directions $\hat{\boldsymbol{b}}_1,\ldots,\hat{\boldsymbol{b}}_6$. By transmission to a neighboring cell, the helicity of the photon path changes and with it the step lengths.

B. Angle of incidence: $\varphi=30°$

For completely reflecting edges, the photons move along a closed path again composed of six steps (see Fig. 3). The three step vectors, $\boldsymbol{b}_i=b\hat{\boldsymbol{b}}_i$ $(i=1,2,3)$, and their reversed partners, $\boldsymbol{b}_i=b'\hat{\boldsymbol{b}}_i$ $(i=4,5,6)$ generally possess different step lengths b and b', which depend on the starting position x_0 on the edge. The average, however, is always the same: $(b+b')/2=\sqrt{3}/2$.

In the central cell of Fig. 3, the photon is always reflected to the left. As before, for partially reflecting edges ($r<1$), the photons move to a neighboring cell, where they are reflected to the right. In the preceding section, we introduced the helicity $\pm$ to distinguish between the two cases. In addition, after transmission to a neighboring cell, the step vectors along one direction interchange their lengths (see Fig. 3). We take this into account by introducing step vectors $\boldsymbol{b}_i^+$ and $\boldsymbol{b}_i^-$.

As before, we introduce the probability $P_n^{\pm i}(\boldsymbol{x})$ that the photon after its nth step arrives at position $\boldsymbol{x}$ with step vector $\boldsymbol{b}_i^{\pm}$ and establish a set of 12 master equations from which we only give the first two ones

$$P_{n+1}^{+1}(\boldsymbol{x}) = rP_n^{+6}(\boldsymbol{x}-\boldsymbol{b}_1^+) + tP_n^{-1}(\boldsymbol{x}-\boldsymbol{b}_1^+),$$

$$P_{n+1}^{-1}(\boldsymbol{x}) = rP_n^{-4}(\boldsymbol{x}-\boldsymbol{b}_1^-) + tP_n^{+1}(\boldsymbol{x}-\boldsymbol{b}_1^-). \qquad (20)$$

Applying the same formalism as in the preceding section, we find again that in the long-time limit the photon moves diffusively with the diffusion constants

$$D(30°) = D_x(30°) = D_y(30°) = \frac{\sqrt{3}}{2}\frac{1-r}{r}lc, \qquad (21)$$

independent of the starting position x_0 on the edge. Interestingly, they agree with the diffusion constant $D(90°)$ for $\varphi = 90°$ introduced in Eq. (2) for the one-dimensional random walk.

We note that $D(30°)$ is larger than $D(60°)$ from Eq. (19) by a factor of $\sqrt{3}$. We roughly understand this as follows. In the case $\varphi = 30°$, the photons are reflected into the forward direction, i.e., their direction changes by a total angle of only 60°. For $\varphi = 60°$ they are reflected in the backward direction, since the direction changes by 120°. In the latter case, the diffusion is therefore much more hindered which leads to a smaller diffusion constant.

IV. NUMERICAL SIMULATIONS

To access the photon's random walk for injection angles different from 30°, 60°, and 90°, we further studied our model by numerical simulations. The computer program takes 10^4 photons at the initial position x_0 (on one of the edges of the hexagon) and with an injection angle φ. Then it generates the trajectory of each photon following a standard Monte Carlo procedure and evaluates the statistics of the photon cloud at times $\tau \in [500,650,\ldots,4850]$ (in units of l/c). The mean-square displacement measuring the width of the photon cloud is computed for each snapshot at time τ and then fitted to $2D\tau + a_0$ for each spatial direction by the method of linear regression. An offset a_0 takes into account the initial ballistic regime. Within our statistical errors, D_x and D_y give the same result and the correlation factor

$$\rho = \frac{\langle xy\rangle - \langle x\rangle\langle y\rangle}{\sqrt{\langle x^2\rangle\langle y^2\rangle}} \qquad (22)$$

is not significant, so the diffusion is isotropic.

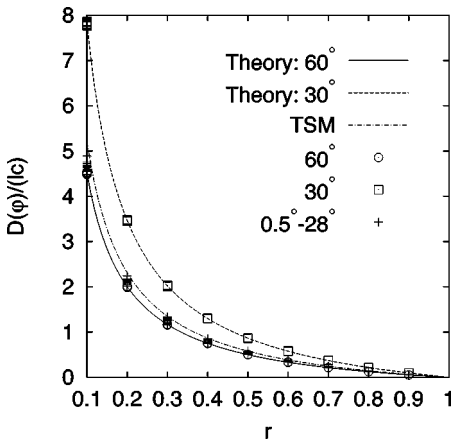

FIG. 4. The diffusion constant in units of edge length l times light velocity c as a function of intensity reflectance r. Theoretical and Monte Carlo simulation results are denoted, respectively, by lines and points. The dash-dotted line refers to the two-state model (TSM).

For angles $\varphi = 30°$, 60° and values between 0° and 30°, the simulation is repeated for each intensity reflectance $r \in [0.1,0.2,\ldots,0.9]$ with all values of $x_0 \in [0.05,0.1,\ldots,0.9]$. In Fig. 4 we plot the average of the diffusion constants D_x and D_y as a function of r. The diffusion constants at $\varphi = 60°$ (open circles ○) and $\varphi = 30°$ (open boxes □) are shown for all values of the starting point x_0. The numerical results agree very well with the theoretical values of Eqs. (19) and (21) for the diffusion constants. The relative error of the numerical values with respect to the theoretical prediction is less than 2% and within our statistical error. No dependence on the starting point x_0 is observed in agreement with theory.

The diffusion constants for angles between 0.5° and 28° (plus symbol +) all lie close to $D(60°)$. A careful inspection shows that they are situated above the 60° line. Furthermore, our statistical errors reveal that the deviation from the 60° line is significant. To investigate this observation further, we performed a series of simulations for the angular ranges $\varphi \in [0.5°,6.4°,\ldots,24.1°]$, $\varphi \in [25°,26°,\ldots,29°]$, and $\varphi \in [29.1°,29.2°,\ldots,29.9°]$. To increase the resolution, the rescaled diffusion constant $D(\varphi)/D(\varphi = 60°)$ versus r is plotted in Fig. 5. We have averaged $D(\varphi)$ over all starting positions x_0. The errorbars shown for $\varphi = 0.5°$ reflect the standard deviation of this averaging process. The errorbars are similar for all the other points.

Figure 5 reveals several remarkable features. Angles close to $\varphi = 0°$ are associated with angles close to 60°, as explained in Sec. II. So the diffusion constant is close to $D(60°)$ as demonstrated by the full line. Increasing now the incident angle from $\varphi = 0°$ to $\varphi = 30°$ results in a systematic increase of the diffusion constant. However, for $\varphi \to 30°$, we do not obtain the result $D(30°)/D(60°) = \sqrt{3}$ as one might expect. Instead the ratio $D(\varphi)/D(60°)$ converges against a value between 1.15 and 1.16. Though the calculation of $D(\varphi)$ is beyond any theoretical treatment, we succeeded to treat the limiting case of $\varphi \to 30°$ analytically in a two-state model which we present in the following section. The result

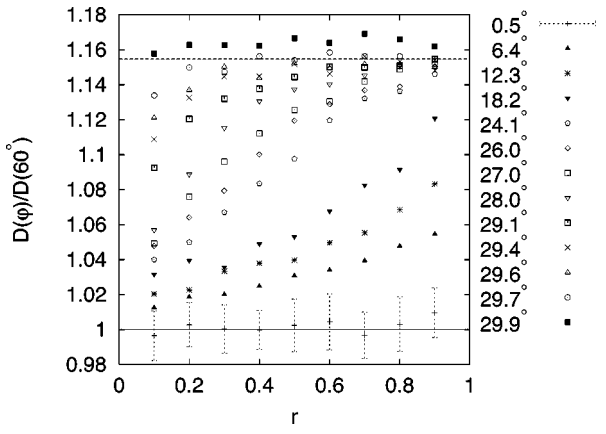

FIG. 5. The diffusion constant $D(\varphi)$ plotted relative to $D(60°)$ as a function of intensity reflectance r for different values of injection angle φ. The dashed line is the limiting case $D(\varphi \to 30°)$ calculated within the two-state model in Sec. V.

is already indicated as dashed line in Fig. 5 and also in Fig. 4. In addition, Fig. 5 demonstrates that $D(\varphi)$ systematically deviates from the simple $(1-r)/r$ law calculated for the analytic cases.

We started to investigate disordered foams. In an imperfect honeycomb structure with slightly random disorder, the special case for $\varphi = 30°$ does no longer exist, as expected. Furthermore, all the curves in Fig. 5 for different injection angles collapse on a single curve, i.e., the diffusion constant no longer depends on φ. However, the surprising result is that the diffusion constant still deviates from the usual $(1-r)/r$ law since it contains an additional factor linear in r. So one special feature of Fig. 5 is preserved. We can explain this behavior within an effective cage model. Details will be reported in a forthcoming paper [27].

V. TWO-STATE MODEL

In Sec. II we explained that the incident angles $\varphi_1 = \varphi_2 = 30°$ and $\varphi_3 = 90°$ correspond to separate random walks in two and one dimension. However, if φ_1 deviates slightly from 30°, the two random walks mix as illustrated in Fig. 6

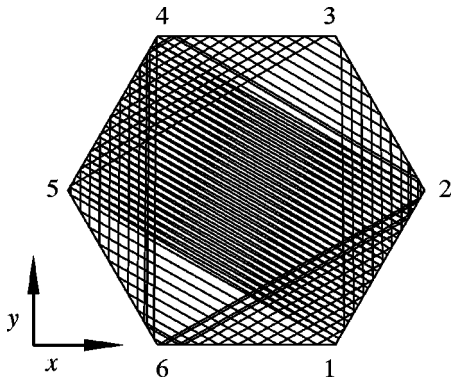

FIG. 6. Path of a photon injected with an angle $\varphi = 29.4°$ relative to the bottom edge of the hexagonal billiard. The photon circles in the hexagon until it switches to a one-dimensional bouncing state between the edges 12 and 45.

for $r = 1$. That means the motion of the photon consists of two different states. In the first one it spends some time τ_{2d} diffusing in the plane. Then it switches to the second state where it performs essentially a one-dimensional random walk, bouncing between two opposite edges during the time τ_b, until it switches back to the previous state. In the theory of random walks such a process is described by a multistate formalism [17]. It calculates the diffusion constant for the two-state process as an average of the diffusion constant for the single states weighted by the average waiting times τ_{2d} and τ_b, the random walker spends in each state,

$$D_x(\varphi \to 30°) = \frac{D_x(30°)\tau_{2d} + D_{bx}\tau_b}{\tau_{2d} + \tau_b}, \tag{23a}$$

$$D_y(\varphi \to 30°) = \frac{D_y(30°)\tau_{2d} + D_{by}\tau_b}{\tau_{2d} + \tau_b}. \tag{23b}$$

The effective diffusion constants for the bouncing state, D_{bx} and D_{by}, can be related to $D(90°)$ as follows. We assume that all three possible bouncing states between opposite edges occur with the same probability. Furthermore, their contributions to D_{bx} and D_{by} are obtained by projecting the one-dimensional random walk onto the x and y direction, which finally gives

$$D_{bx} = \tfrac{2}{3}\cos^2 30° D(90°) = \tfrac{1}{2}D(90°), \tag{24a}$$

$$D_{by} = \tfrac{1}{3}(2\sin^2 30° + 1)D(90°) = \tfrac{1}{2}D(90°). \tag{24b}$$

The calculation of the waiting times is a geometrical exercise. Let us consider first the bouncing state which the photon enters at the lower right corner 1 of the hexagon in Fig. 6. It then travels along the diagonal hitting the opposite edge 45, a small distance δs_b away from the corner 5. In successive reflections or transmissions, the photon's position moves along the edge until it hits either the corner 2 or 4. Here the photon switches to the two-dimensional state. In our reduced units, the number of steps n_b in the bouncing state is thus approximated by $1/\delta s_b$. Multiplied with the step time $\delta\tau_b$, gives the waiting time

$$\tau_b = n_b \delta\tau_b, \tag{25}$$

with

$$n_b = \frac{1}{\sqrt{3}\tan(30° - \varphi)} \quad \text{and} \quad \delta\tau_b = \frac{\sqrt{3}}{\cos(30° - \varphi)}. \tag{26}$$

In the two-dimensional random walk, the photon takes a short and a long step to move a distance δs_{2d} along the edge. The waiting time τ_{2d} is then calculated from the number of steps n_{2d} and the step time $\delta\tau_{2d}$ as

$$\tau_{2d} = n_{2d}\delta\tau_{2d}, \tag{27}$$

with

$$n_{2d}=\frac{2\sin\varphi}{\sqrt{3}\sin(30°-\varphi)} \quad \text{and} \quad \delta\tau_{2d}=\frac{\sqrt{3}}{4\sin\varphi}. \tag{28}$$

It is the ratio τ_{2d}/τ_b which enters the effective diffusion constants. Using Eqs. (25)–(28) gives $\tau_{2d}/\tau_b=1/2$. The ratio is independent of φ due to our approximation for n_b and n_{2d}. It becomes exact for $\varphi\to 30°$. Together with Eqs. (24) and the actual values for $D(30°)$ [Eq. (21)] and $D(90°)$ [Eq. (2)], we obtain from Eqs. (23)

$$D_x(\varphi\to 30°)=D_y(\varphi\to 30°)=\frac{\sqrt{3}}{3}\frac{1-r}{r}lc. \tag{29}$$

This is the value indicated in Fig. 5 relative to $D(60°)$ as dashed line. The limiting value of $\tau_{2d}/\tau_b=1/2$ means that there is no smooth transition to $D(30°)$ for $\varphi\to 30°$.

VI. CONCLUSIONS

We have studied a persistent random walk on a honeycomb structure based on rules motivated by geometric optics. Both analytical and numerical studies confirm the diffusive behavior of the photons in the long-time limit. Three cases of the injection angle, $\varphi=30°$, 60°, and 90°, allow an analytic expression for $D(\varphi)$ from which the third one for a one-dimensional persistent random walk is well known in literature. The second and third case can be solved although they correspond to a Markov chain of 12th order. In all three cases, the diffusion constant is proportional to $(1-r)/r$ which expresses the fact that for $r=0$ the photon transport is ballistic and that for $r=1$ the photon stays confined to the initial hexagon. Numerical simulations demonstrate an interesting dependence of the diffusion constant on the injection angle φ summarized as $D(60°)<D(\varphi)<D(\varphi\to 30°)<D(30°)$, where $D(60°)$ and $D(\varphi\to 30°)$ differ by a factor of $2\sqrt{3}/3$. This is a remarkable property since usually the diffusion process erases the memory for the initial conditions. The numerical results of $D(\varphi)$ reveal a fourth analytically solvable case for injections angles $\varphi\to 30°$, where the motion of the photon switches between a one- and two-dimensional diffusion state. Accordingly, the random walk is described within a two-state model. In addition, the simulations show a significant deviation from the simple $(1-r)/r$ law of the analytic cases for which we do not have any explanation so far.

In light transport the transport-mean-free path l^* plays a determining role since it is a measure for the length over which the direction of propagation has fully changed [1]. In two-dimensional systems, it is defined via $D=cl^*/2$. As a key parameter, it can be measured experimentally [4–6]. In our case it is of the order of $(1-r)l/r$. In a realistic model for r based on the Fresnel formulas and for thicknesses d of the liquid films comparable to the wavelength of light, we find a significant dependence on incident angle φ and d [27]. When averaged over φ and d, we obtain $r\approx 0.2$ which gives realistic values of $l^*\approx 4l$ [10].

Of course, our model is highly simplified. We therefore have extended our studies towards real foams by introducing topological and geometrical disorder based on a Voronoi foam model [15]. In addition, as just mentioned, we have implemented the exact intensity reflectance r using the Fresnel formulas. Furthermore, we have introduced disorder in the film thickness. The results will be presented elsewhere [27]. A possible extension of our model might include scattering from the Plateau borders as suggested in Ref. [10].

ACKNOWLEDGMENTS

We would like to thank S. Cohen-Addad, R. Höhler, H. Larralde, G. Maret, N. Rivier, S. E. Skipetrov, D. Weaire, and J. Wiersig for fruitful discussions. H.S. acknowledges financial support from the Deutsche Forschungsgemeinschaft under Grant No. Sta 352/5-1. MF.M. thanks the International Graduate College at the University of Konstanz for financial support.

APPENDIX

The matrix $\boldsymbol{M}$, introduced in Eq. (8), can conveniently be written in block form

$$\boldsymbol{M}=\begin{pmatrix} \mathbf{0} & t\boldsymbol{M}_1 & \mathbf{0} & \mathbf{0} & r\boldsymbol{M}_1 & \mathbf{0} \\ t\boldsymbol{M}_1 & \mathbf{0} & \mathbf{0} & r\boldsymbol{M}_1 & \mathbf{0} & \mathbf{0} \\ r\boldsymbol{M}_2 & \mathbf{0} & \mathbf{0} & t\boldsymbol{M}_2 & \mathbf{0} & \mathbf{0} \\ \mathbf{0} & \mathbf{0} & t\boldsymbol{M}_2 & \mathbf{0} & \mathbf{0} & r\boldsymbol{M}_2 \\ \mathbf{0} & \mathbf{0} & r\boldsymbol{M}_3 & \mathbf{0} & \mathbf{0} & t\boldsymbol{M}_3 \\ \mathbf{0} & r\boldsymbol{M}_3 & \mathbf{0} & \mathbf{0} & t\boldsymbol{M}_3 & \mathbf{0} \end{pmatrix}, \tag{A1}$$

where

$$\mathbf{0}=\begin{pmatrix} 0 & 0 \\ 0 & 0 \end{pmatrix},$$

$$\boldsymbol{M}_n=\begin{pmatrix} 0 & \exp(i\boldsymbol{k}\cdot\boldsymbol{b}_{nl}) \\ \exp(i\boldsymbol{k}\cdot\boldsymbol{b}_{ns}) & 0 \end{pmatrix}. \tag{A2}$$

The characteristic equation of $\boldsymbol{M}$ reads

$$\det(\boldsymbol{M}-z\mathbf{1})=\sum_{i=0}^{i=6} m_{2i}z^{2i}=0, \tag{A3}$$

where

$$m_{12}=1,$$

$$m_{10}=-2(1-r)^2\sigma_1,$$

$$m_8=2(1-r)^2(r^2-4r+2)\sigma_1^*+(1-r)^4\sigma_2,$$

$$m_6=2(1-r)^4(-1+2r)\sigma_3-2(4-24r+54r^2-56r^3+27r^4-6r^5+2r^6),$$

$$m_4=(1-2r)^2(1-r)^4\sigma_2^*+2(2-4r+r^2)(1-3r+2r^2)^2\sigma_1,$$

$$m_2 = -2(1-2r)^4(1-r)^2\sigma_1^*,$$

$$m_0 = (1-2r)^6, \tag{A4}$$

with

$$\sigma_1 = \exp[i(\boldsymbol{b}_{1l}+\boldsymbol{b}_{1s})\cdot\boldsymbol{k}] + \exp[i(\boldsymbol{b}_{2l}+\boldsymbol{b}_{2s})\cdot\boldsymbol{k}] + \exp[i(\boldsymbol{b}_{3l}+\boldsymbol{b}_{3s})\cdot\boldsymbol{k}],$$

$$\sigma_2 = \exp[2i(\boldsymbol{b}_{1l}+\boldsymbol{b}_{1s})\cdot\boldsymbol{k}] + \exp[2i(\boldsymbol{b}_{2l}+\boldsymbol{b}_{2s})\cdot\boldsymbol{k}] + \exp[2i(\boldsymbol{b}_{3l}+\boldsymbol{b}_{3s})\cdot\boldsymbol{k}],$$

$$\sigma_3 = 2\cos[(\boldsymbol{b}_{1l}+\boldsymbol{b}_{1s}-\boldsymbol{b}_{3l}-\boldsymbol{b}_{3s})\cdot\boldsymbol{k}] + 2\cos[(\boldsymbol{b}_{1l}+\boldsymbol{b}_{1s}-\boldsymbol{b}_{2l}-\boldsymbol{b}_{2s})\cdot\boldsymbol{k}] + 2\cos[(\boldsymbol{b}_{3l}+\boldsymbol{b}_{3s}-\boldsymbol{b}_{2l}-\boldsymbol{b}_{2s})\cdot\boldsymbol{k}]. \tag{A5}$$

The eigenvalues, evaluated at $\boldsymbol{k}=\boldsymbol{0}$, are

$$z_1 = -z_2 = 1,$$

$$z_3 = -z_4 = |2r-1|,$$

$$z_5 = z_6 = -z_7 = -z_8 = -0.5r - 0.5\sqrt{4-8r+r^2},$$

$$z_9 = z_{10} = -z_{11} = -z_{12} = -0.5r + 0.5\sqrt{4-8r+r^2}, \tag{A6}$$

with $|z_i| \leqslant 1$ for $0 \leqslant r \leqslant 1$.

The coefficients introduced in Eq. (17) are evaluated as

$$\frac{\partial^2 S_1}{\partial k_x^2}\Big|_{\boldsymbol{k}=\boldsymbol{0}} = \frac{\partial^2 S_1}{\partial k_y^2}\Big|_{\boldsymbol{k}=\boldsymbol{0}} = 108(1-r)^2 r^4$$

$$S_2|_{\boldsymbol{k}=\boldsymbol{0}} = 72(1-r)r^5, \tag{A7}$$

where

$$S_1 = \sum_{i=1}^{i=5} m_{2i} \quad \text{and} \quad S_2 = \sum_{i=1}^{i=6} 2i \;\; m_{2i}. \tag{A8}$$

[1] *Scattering and Localization of Classical Waves in Random Media* edited by P. Sheng (World Scientific, Singapore, 1990); P. Sheng, *Introduction to Wave Scattering, Localization, and Mesoscopic Phenomena* (Academic Press, San Diego, 1995).

[2] G. Maret, in *Mesoscopic Quantum Physics*, Proceedings of the Les Houches Summer School, Session LXI, 1994, edited by E. Akkermans, G. Montambaux, J.-L. Pichard, and J. Zinn-Justin (North-Holland, Amsterdam, 1995).

[3] B. van Tiggelen and H. Stark, Rev. Mod. Phys. **72**, 1017 (2000).

[4] G. Maret and P.E. Wolf, Z. Phys. B: Condens. Matter **65**, 409 (1987); G. Maret, Curr. Opin. Colloid Interface Sci. **2**, 251 (1997).

[5] D.J. Pine, D.A. Weitz, P.M. Chaikin, and E. Herbolzheimer, Phys. Rev. Lett. **60**, 1134 (1988).

[6] P.D. Kaplan, A.D. Dinsmore, A.G. Yodh, and D.J. Pine, Phys. Rev. E **50**, 4827 (1994).

[7] S. Feng, in *Scattering and Localization of Classical Waves in Random Media*, edited by P. Sheng (World Scientific, Singapore, 1990).

[8] D.J. Durian, D.A. Weitz, and D.J. Pine, Science **252**, 686 (1991).

[9] D.J. Durian, D.A. Weitz, and D.J. Pine, Phys. Rev. A **44**, R7902 (1991).

[10] M.U. Vera, A. Saint-Jalmes, and D.J. Durian, Appl. Opt. **40**, 4210 (2001).

[11] J.C. Earnshaw and A.H. Jaafar, Phys. Rev. E **49**, 5408 (1994).

[12] R. Höhler, S. Cohen-Addad, and H. Hoballah, Phys. Rev. Lett. **79**, 1154 (1997).

[13] S. Cohen-Addad and R. Höhler, Phys. Rev. Lett. **86**, 4700 (2001).

[14] D. Weaire and S. Hutzler, *The Physics of Foams* (Oxford Univerity Press, New York, 1999).

[15] D. Weaire and N. Rivier, Contemp. Phys. **25**, 59 (1984).

[16] H.M. Princen, J. Colloid Interface Sci. **91**, 160 (1983).

[17] G. H. Weiss, *Aspects and Applications of the Random Walk* (North-Holland, Amsterdam, 1994).

[18] J.W. Haus and K.W. Kehr, Phys. Rep. **150**, 263 (1987).

[19] G.I. Taylor, Proc. London Math. Soc. **20**, 196 (1921).

[20] P. J. Flory, *Statistical Mechanics of Chain Molecules* (Interscience, New York, 1969).

[21] M. E. Glicksman, *Diffusion in Solids: Field Theory, Solid-State Principles, and Applications* (Wiley, New York, 2000).

[22] H. Larralde, Phys. Rev. E **56**, 5004 (1997).

[23] M. Boguñá, J.M. Porrà, and J. Masoliver, Phys. Rev. E **58**, 6992 (1998).

[24] M. Boguñá, J.M. Porrà, and J. Masoliver, Phys. Rev. E **59**, 6517 (1999).

[25] P.J. Richens and M.V. Berry, Physica D **2**, 495 (1981).

[26] J. Wiersig, Phys. Rev. E **64**, 026212 (2001); Phys. Rev. A **67**, 023807 (2003).

[27] MF. Miri and H. Stark (unpublished).